NAVAL POSTGRADUATE SCHOOL
Monterey, California

THESIS

INVESTIGATION OF ANOMALOUS CLOUD FEATURES IN
3.7 MICROMETER SATELLITE IMAGERY

by

John M. Rogers

March 1987

Thesis Advisor: P. A. Durkee

Approved for public release; distribution is unlimited

SECURITY CLASSIFICATION OF THIS PAGE

REPORT DOCUMENTATION PAGE

1a REPORT SECURITY CLASSIFICATION: UNCLASSIFIED	1b RESTRICTIVE MARKINGS
2a SECURITY CLASSIFICATION AUTHORITY	3 DISTRIBUTION/AVAILABILITY OF REPORT: Approved for public release; distribution is unlimited
2b DECLASSIFICATION / DOWNGRADING SCHEDULE	
4 PERFORMING ORGANIZATION REPORT NUMBER(S)	5 MONITORING ORGANIZATION REPORT NUMBER(S)
6a NAME OF PERFORMING ORGANIZATION: Naval Postgraduate School; 6b OFFICE SYMBOL (If applicable)	7a NAME OF MONITORING ORGANIZATION: Naval Postgraduate School
6c ADDRESS (City, State, and ZIP Code): Monterey, California 93943-5000	7b ADDRESS (City, State, and ZIP Code): Monterey, California 93943-5000
8a NAME OF FUNDING/SPONSORING ORGANIZATION; 8b OFFICE SYMBOL (If applicable)	9 PROCUREMENT INSTRUMENT IDENTIFICATION NUMBER
8c ADDRESS (City, State, and ZIP Code)	10 SOURCE OF FUNDING NUMBERS: PROGRAM ELEMENT NO; PROJECT NO; TASK NO; WORK UNIT ACCESSION NO

11 TITLE (Include Security Classification)
INVESTIGATION OF ANOMALOUS CLOUD FEATURES IN 3.7 MICROMETER SATELLITE IMAGERY

12 PERSONAL AUTHOR(S)
Rogers, John M.

13a TYPE OF REPORT	13b TIME COVERED	14 DATE OF REPORT (Year, Month, Day)	15 PAGE COUNT
Master's Thesis	FROM ______ TO ______	1987 March	83

16 SUPPLEMENTARY NOTATION

17 COSATI CODES			18 SUBJECT TERMS (Continue on reverse if necessary and identify by block number)
FIELD	GROUP	SUB-GROUP	Clouds, satellite techniques, visible, near-infrared, infrared, radiative transfer, aerosol effects

19 ABSTRACT (Continue on reverse if necessary and identify by block number)

When band 3 (3.7 micrometers) daylight AVHRR imagery are examined, unique effects not present in the other four bands are observed. These effects include a higher radiance from cloud tops than from the sea-surface, unique ship exhaust tracks and the highlighting of areas of thin clouds, continental aerosol intrusion into marine air and ice clouds. These effects are due to the addition of various amounts of reflected solar radiance and thermal emitted radiance. In this thesis, three cases illustrating these effects are examined.

The apparent temperature reversals result from clouds reflecting more solar radiation than the sea surface. Ship tracks and continental aerosol effects are due to altered size distributions caused by added ship exhaust pollutants or aerosols. The absorptivity of ice clouds is higher than

20 DISTRIBUTION/AVAILABILITY OF ABSTRACT: ☒ UNCLASSIFIED/UNLIMITED ☐ SAME AS RPT ☐ DTIC USERS	21 ABSTRACT SECURITY CLASSIFICATION: UNCLASSIFIED
22a NAME OF RESPONSIBLE INDIVIDUAL: P. A. Durkee	22b TELEPHONE (Include Area Code): (408) 646-3465; 22c OFFICE SYMBOL: 63De

DD FORM 1473, 84 MAR 83 APR edition may be used until exhausted. All other editions are obsolete

SECURITY CLASSIFICATION OF THIS PAGE

Block 19 continued
water clouds, thus the sensed radiance from ice clouds is essentially only emitted, not reflected. Therefore, ice clouds appear colder than liquid water clouds in band 3.

Approved for public release; distribution is unlimited.

Investigation of Anomalous Cloud Features in 3.7 Micrometer Satellite Imagery

by

John M. Rogers
Captain, United States Air Force
B. S., Metropolitan State College, 1982

Submitted in partial fulfillment of the requirements for the degree of

MASTER OF SCIENCE IN METEOROLOGY

from the

NAVAL POSTGRADUATE SCHOOL
March 1987

ABSTRACT

When band 3 (3.7 micrometers) daylight AVHRR imagery are examined, unique effects not present in the other four bands are observed. These effects include a higher radiance from cloud tops than from the sea-surface, unique ship exhaust tracks and the highlighting of areas of thin clouds, continental aerosol intrusion into marine air and ice clouds. These effects are due to the addition of various amounts of reflected solar radiance and thermal emitted radiance. In this thesis, three cases illustrating these effects are examined.

The apparent temperature reversals result from clouds reflecting more solar radiation than the sea surface. Ship tracks and continental aerosol effects are due to altered size distributions caused by added ship exhaust pollutants or aerosols. The absorptivity of ice clouds is higher than water clouds, thus the sensed radiance from ice clouds is essentially only emitted, not reflected. Therefore, ice clouds appear colder than liquid water clouds in band 3.

TABLE OF CONTENTS

I. INTRODUCTION

The National Oceanographic and Atmospheric Administration (NOAA) polar orbiting weather satellites use an Advanced Very High Resolution Radiometer (AVHRR), among other sensors, to observe the earth. The AVHRR observes a swath of the earth's surface in five individual wavelength bands, with a resolution of about 1 km. The wavelengths and wavenumbers of the bands are given in Table 1. Band 1 is in the visible wavelength region. Band 2 is in the very-near infrared (IR) wavelength region and most objects imaged by band 2 appear similar to band 1. The imagery are processed so areas of high radiance are bright and areas of low radiance are dark. Thus, water looks dark and clouds appear white. However, land features have higher band 2 reflectivities than band 1 reflectivities. Therefore, a higher percentage of band 2 radiation is reflected than band 1 radiation. Thus, land surfaces appear lighter and have more detail in band 2 imagery than in band 1 imagery. Figs. 1 and 2 are examples of band 1 and band 2 imagery.

Bands 4 and 5 sense radiance in the thermal IR window region. Therefore, the imagery of bands 4 and 5 imply relative temperatures. Low radiance (low temperature) pixels are bright and high radiance (higher temperature)

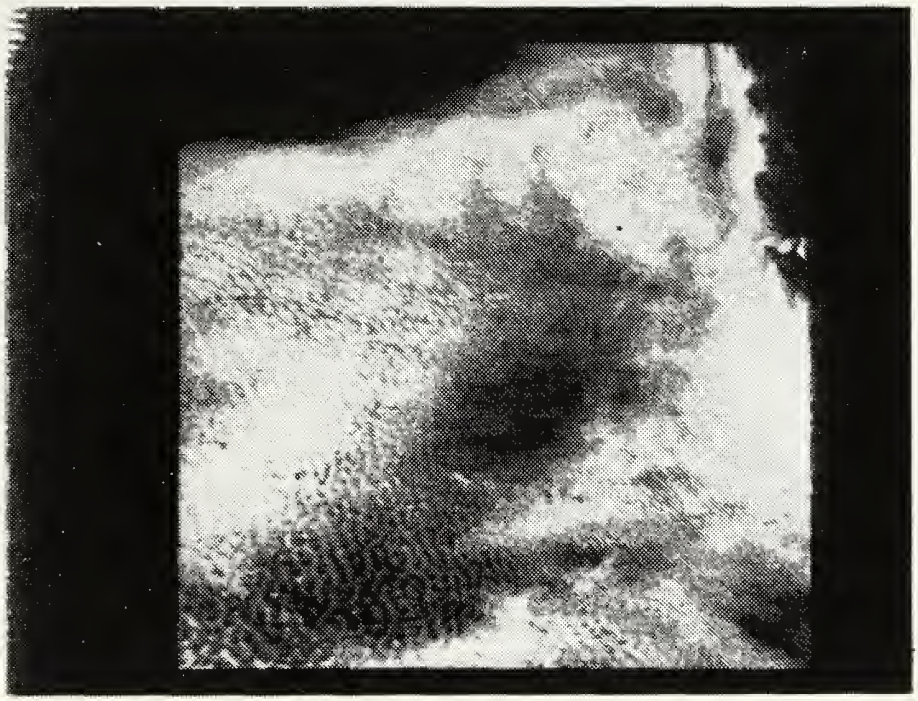

Fig. 1. AVHRR band 1 image, 1400 LST, 3 April 1987 off the coast of southern California.

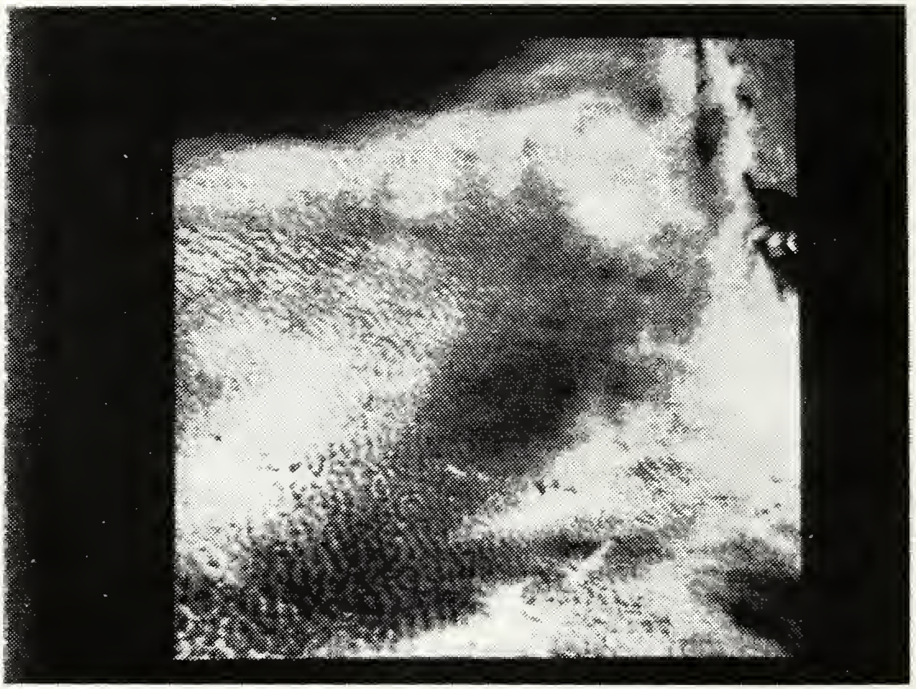

Fig. 2. Same as Fig. 1, band 2 image.

pixels are dark. Clouds, especially high clouds, are usually much colder than underlying surfaces. However, very low clouds may be nearly the same temperature as the underlying surface. Therefore, the display convention for bands 4 and 5 yields white, high clouds against a grey ocean surface. Very low clouds, such as fog and low stratus, may be nearly indistinguishable from the adjacent surfaces with similar temperatures. See Figs. 3 and 4 for examples of bands 4 and 5 imagery.

TABLE 1

AVHRR BANDS (Kidwell, 1984)

Band	Wavelengths (micrometers)	Wavenumbers (per centimeter)
1	0.58 - 0.68	14,700 - 17,200
2	0.75 - 1.10	9,090 - 13,300
3	3.55 - 3.93	2,540 - 2,820
4	10.50 -11.30	885 - 952
5	11.50 -12.50	800 - 870

Band 3 senses radiance near the boundary of the near infrared and thermal infrared regions. During daytime observations the sensed radiance is composed of both emitted thermal and reflected solar radiation. Band 3 imagery are displayed the same way as band 4 and 5 imagery; low radiance

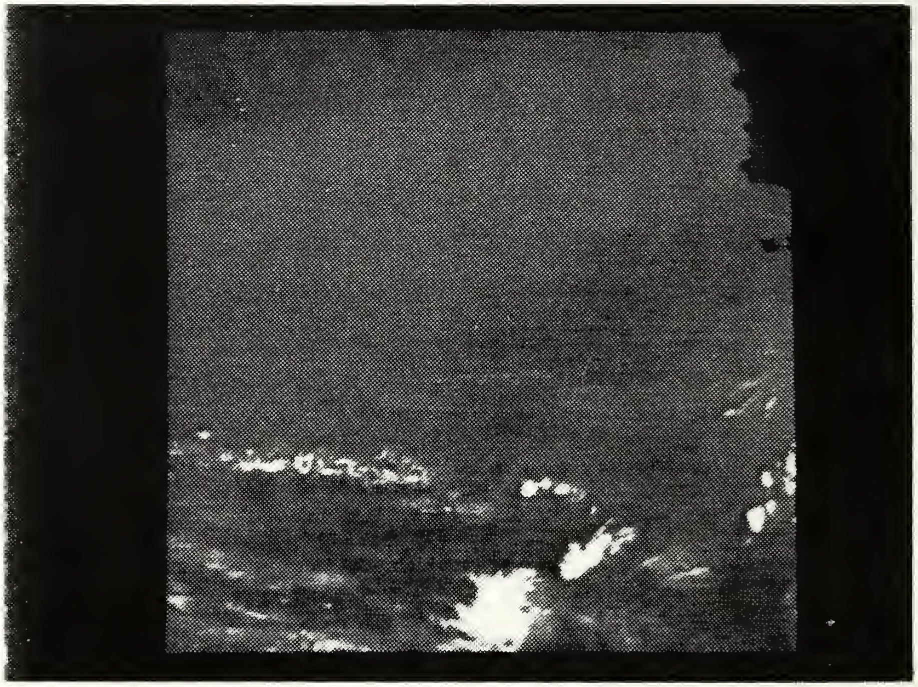

Fig. 3. Same as Fig. 1, band 4 image.

Fig. 4. Same as Fig. 1, band 5 image.

(brightness) pixels are bright and high radiance (brightness) pixels are dark. In night time imagery, the imagery generally displays light clouds against a darker background.

Two types of phenomena that are unique to band 3 imagery will be discussed here. The first, as reported by Bell and Wong (1981), is the apparent reversal of cloud top and sea-surface temperatures in daylight band 3 imagery. This results in dark clouds against a lighter ocean surface.

The second feature consists of anomalous lines that do not appear to be associated with any geographical or meteorological source. The lines generally are not apparent on the associated bands 1, 2, 4 or 5 imagery. They may cross each other, occur parallel to each other, or be isolated. The streaks are apparently caused by the exhaust plumes of ships passing through the area. The streaks will be referred to as "ship tracks." Ship tracks in band 1 and 2 are well known phenomena. Conover (1969) and others have reported visible ship tracks consisting of wide (25 km) stratus bands produced by ship exhaust. See Fett _et al_ (1977) for an excellent review of this phenomenon. However, the anomalous ship tracks discussed in this thesis are not apparent in bands 1, 2, 4 or 5.

Fig. 5 displays a band 3 image that have both a temperature reversal (of cloud tops and sea surface) and

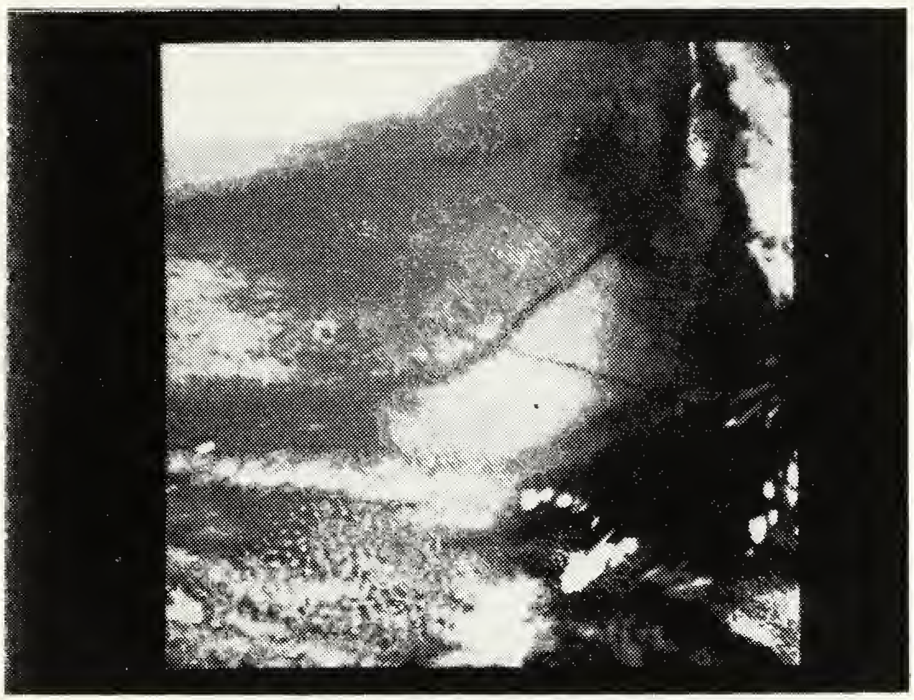

Fig. 5. Same as Fig. 1, band 3 image.

ship tracks. Figs. 1 through 5 are all of the same area and time. The land surface in the top right corner (best visible in the band 4 and 5 imagery in Figs. 3 and 4) is California. Point Conception is located where the coast line changes from a north/south to a west/east orientation.

Fig. 6 is a band 1 overview of the area containing the band 1 through 5 images. The overview area is a full pass of AVHRR imagery of the North Pacific Ocean off the west coast of North America from Baja California to Oregon (which is obscured by high clouds). The full 1 km resolution images (Figs. 1 through 5) are 512 by 512 pixel subscenes of the full pass image. The imagery were recorded on 3 April 1985, at about 1400 LST. Note the cloud/sea boundary at the top left of the band 1 and 2 imagery (Figs. 1 and 2). In bands 4 and 5 (Figs. 3 and 4) the boundary is still present, but has much less contrast. This indicates that the sea surface and cloud tops have nearly the same temperature. The clouds are slightly lighter than the sea surface, indicating they are colder than the sea surface. However, in band 3 (Fig. 5), the sea surface is much lighter than clouds. This would indicate (in night imagery) that the cloud tops are much warmer than the sea surface. This thesis will show the temperature reversals result from reflected solar radiation added to emitted terrestrial radiation.

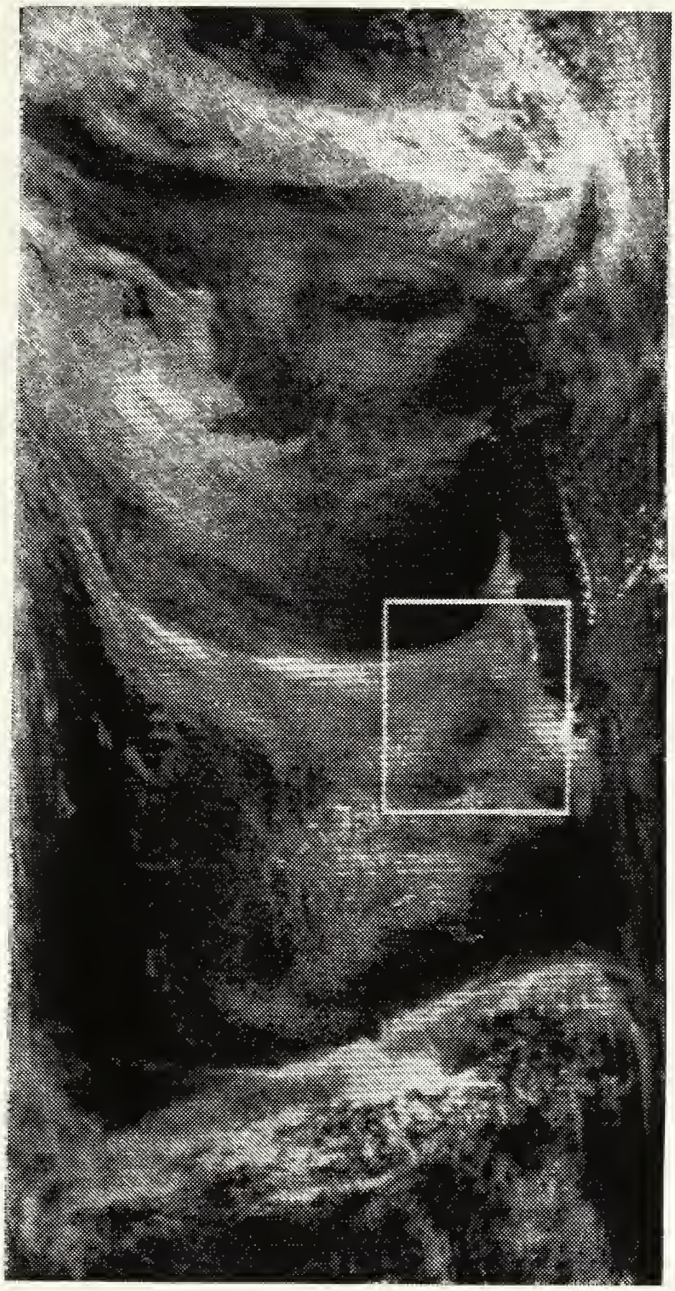

Fig. 6. Same as Fig. 1. Band 1 overview of area. Full resolution image area indicated by box.

Prominent ship tracks are also visible in the center of the band 3 imagery (Fig. 5). Bands 1 and 4 (Figs. 1 and 3) indicate that this is an area of thin, low clouds. There appears to be no evidence suggesting the existance of the ship tracks in the other AVHRR bands (Figs. 1, 2, 3 or 4). A paper is being prepared by Coakley, Bernstein and Durkee describing the anomalous band 3 ship tracks.[1]

An analysis of band 3 imagery will be done by subtracting the band 3 emitted radiances from the individual pixels. These values are calculated from the pixel temperatures derived from band 4 pixel radiances. The result will be an estimate of the reflected band 3 radiances. Finally, the band 3 pixel albedos, from the reflected radiance values, will be divided by the band 2 pixel albedos to highlight the unique features of band 3 imagery relative to band 2.

This thesis will describe the basic reasons for the brightness patterns in bands 1, 2, 4 and 5 imagery. It will then discuss how these factors relate to the band 3 imagery. Chap. III discusses the unique band 3 characteristics that result in the anomalous band 3 features. Then the algorithm used to analyze the imagery will be discussed, followed by

---

[1]Private communication: J. A. Coakley, National Center for Atmospheric Research, Boulder, CO; R. Bernstein, Sea Space, San Diego, CA; and P. A. Durkee, Naval Postgraduate School, Monterey, CA.

a discussion of the specific imagery studied. Specific features in the imagery will be examined and will be related to and illustrate the physical mechanisms described in Chap. II and III.

II. CAUSES OF THE APPEARANCE OF BAND 1, 2, 4 AND 5 IMAGERY

A. BASIC PROCESSES

Electromagnetic radiation is emitted from all physical substances. The amount of radiation emitted is proportional to the emissivity of the substance. The emissivity is a function of the specific substance, its chemistry and physical configuration, and the wavelength (or frequency or wavenumber) of the emitted radiation. A substance that has an emissivity of 1 at all wavelengths is called a black body. As discussed below, clouds act as black bodies at some wavelengths (but not at all wavelengths). According to Kirchoff's law, a body's emissivity at a given wavelength is equal to its absorptivity (the percentage of incident radiation at a given wavelength that a body absorbs). The sun's emissivity at all wavelengths important to this paper is nearly 1. Various features on the earth and in the atmosphere have emissivities from less than 0.05 to nearly 1 at the wavelengths of interest.

The amount of radiation emitted by a black body is given by the Planck function. The Planck function, for a given wavelength and absolute temperature T, is given by

$$B(\lambda,T) = \frac{2hc^2}{\lambda^5 \ (\exp(hc/k\lambda T) - 1)}, \qquad (1)$$

where B = emitted radiance, λ = the wavelength, T = the absolute temperature of the substance, h = the Planck constant, c = speed of light, and k = Boltzmann's constant. Study of Planck's function shows that at a given wavelength more energy is emitted as the temperature rises and also, at a given temperature, there is a wavelength of maximum emitted radiance. Fig. 7 (from Sellers, 1965) shows the solar radiation received at the earth and the radiation emitted from the earth. Solar radiation has a maximum value at a shorter wavelength than the earth's maximum wavelength. The solar radiance at the earth is reduced by a factor of about 220,000 because of the distance from the sun to the earth.

Since the earth's atmospheric features have temperatures from roughly 200 K to 300 K, they emit maximum radiance at wavelengths from 14.5 to 9.66 micrometers. These peaks occur within the infrared (IR) wavelengths. The emitted radiance falls off rapidly at wavelengths shorter than the peak and more slowly at longer wavelengths (as in Fig. 7). Therefore, the earth effectively does not emit radiance in the visual wavelengths from about 0.4 to 0.7 micrometers.

The sun has a surface temperature of about 6000 K, thus its wavelength of peak radiance is about 0.48 micrometers. This peak is within the visible wavelengths. It emits much more IR radiation than does the earth. However, due to the large sun to earth distance, the solar IR radiance in bands

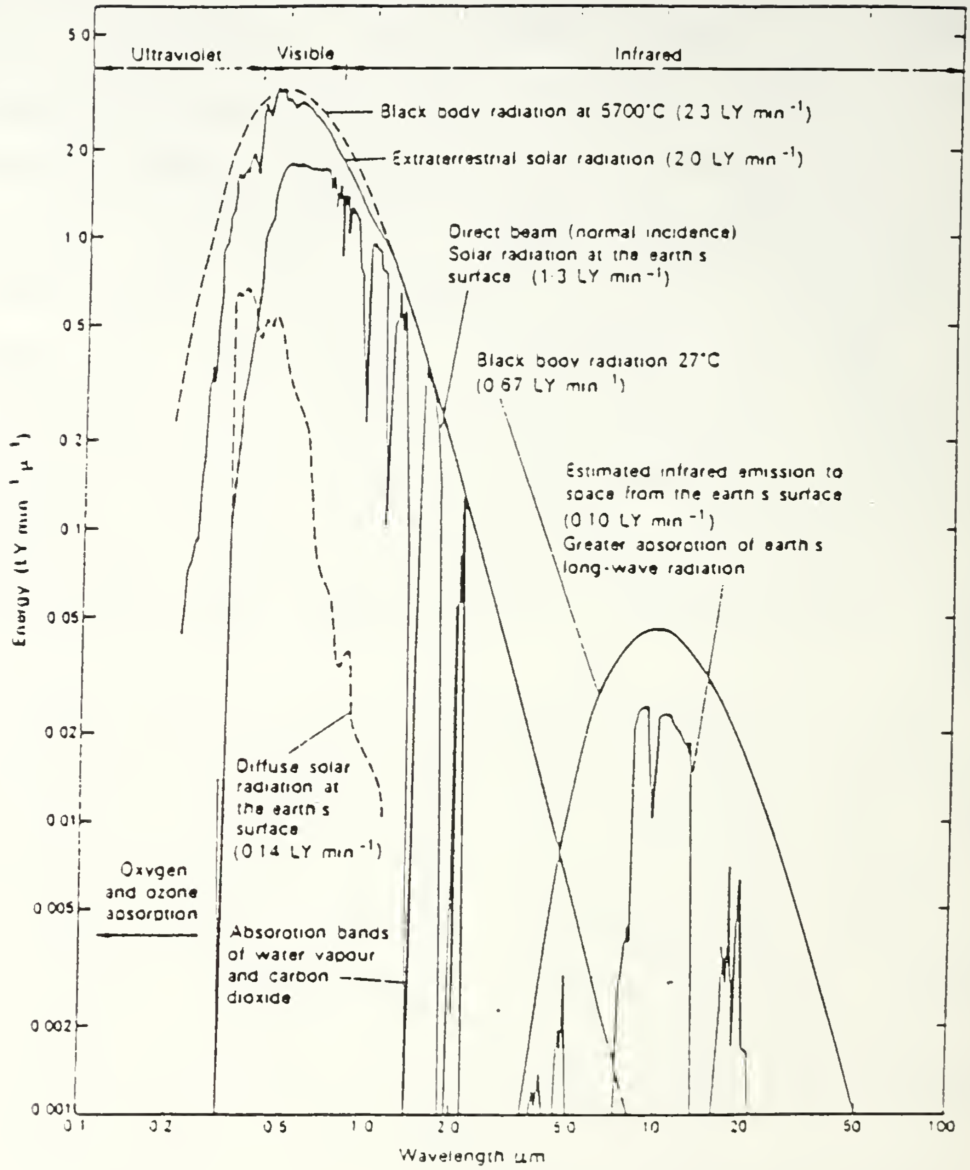

Fig. 7. Electromagnetic solar radiance received at the top of the earth's atmosphere and earth's thermally emitted radiation. The black body curves for the sun and earth are indicated by the smooth curves (from Sellers, 1965).

4 and 5 received at the earth is much less than the earth's emitted IR radiance, as is shown in Fig. 7.

Radiation encountering atmospheric constituents (air molecules, dust particles, pollutants, or cloud, rain, snow or ice particles) will be affected in one or more of three ways. It may be transmitted through, scattered by or absorbed by the constituents. Scattering mechanisms result in reflection of radiation by clouds, giving clouds their bright white visual appearance.

Scattering is given by

$$b = \int_0^\infty \pi r^2 n(r) Q(m,r) dr, \qquad (2)$$

where b is the total scattering in a thin (dz), horizontal section of the atmosphere, r is the radius, r^2 is the cross sectional area of the droplets, m is the index of refraction, Q(m,r) is the scattering efficiency, and n(r) is the size distribution of the droplets (after Bohren and Huffman, 1983). The scattering efficiency of the particles is related to the size of the particles compared to the wavelength of the radiation. If the particles are much larger than the wavelength of the radiation, their scattering efficiency is independent of their size and is equal to about 2.

If the particle radius and the wavelength are comparable, the scattering is more complicated and is

described by Mie theory. The resulting scattering efficiencies are described, in part, by a variable x, where

$$x = 2\pi r/\lambda \quad . \qquad (3)$$

The scattering efficiency curve for water droplets is given by Friedlander (1977) as in Fig. 8. Note that at the large values of x the scattering efficiency is approaching 2.

Finally, if the particles are much smaller than the wavelength of the radiation, scattering is more simply described by Rayleigh scattering. Rayleigh scattering is much less efficient than Mie scattering. The extinction efficiency is proportional to the fourth power of x (Bohren and Huffman, 1983.) The Rayleigh scattering region is where the scattering efficiency is small, i.e. $x < 1$.

B. SPECIFIC EFFECTS

Band 1 radiance (around 0.6 micrometers) is almost exclusively due to solar radiation. There is, effectively, no emission of 0.6 micrometer radiation at terrestrial temperatures. Table 2 compares the calculated radiances at the center of bands 1, 3 and 4 that are received at the earth from the sun and that are emitted by a black body at 280 K. The solar emission has a peak value between 0.45 and 0.50 micrometers (Thekaekare et al., 1969.) Therefore, essentially all 0.6 micrometer radiation received by a

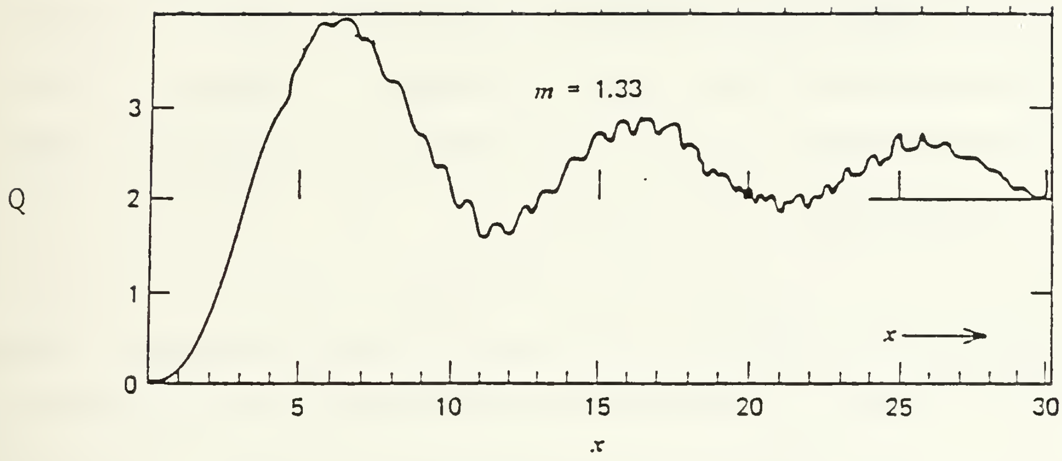

Fig. 8. Extinction curve for water spheres calculated from Mie theory (from Friedlander, 1977). Q and x are dimensionless.

satellite from the earth is reflected or scattered solar radiation. Except for the area of sun glint (the area of specular reflection off the surface of the ocean) the ocean absorbs most of the incoming 0.6 micrometer solar radiation.

TABLE 2

CALCULATED RADIANCES

(in W/m^2 sr cm)

Wavelength (micrometers)	0.63	3.7	11.0
Received from sun	5.16e6	38900	632
Emitted from earth (at 280 K)	4.52e-23	1600	6990

According to Coakley and Davies (1985), 0.63 micrometer albedos for 500 m thick stratus and nimbostratus clouds are 0.55 and 0.83, respectively, while the albedo of the sea surface is less than 5%. If a standard 0.63 micrometer solar irradiance is assumed, the clouds will scatter 10 to 15 times as much radiance back to the satellite as the ocean surface. Therefore, the clouds will appear much brighter than the ocean surface away from the sun glint area. In bands 1 and 2 (Figs. 1 and 2), clouds cover most of the ocean. An area of the ocean is in the northwest corner with an area of scattered clouds in the center.

Barrett _et al._, (1979) measured water droplets in marine stratus clouds and found a mean radius of about 4

micrometers. Stratus clouds containing urban pollution were measured to have a mean droplet radius of about 3 micrometers. The size distributions (n(r), or the number of droplets per radius per unit volume) for these different cloud types are shown in Fig. 9. This thesis proposes that the ship tracks observed in band 3 images are the result of the injection of pollutants into cloud areas by ships' exhaust, thus altering the droplet size distribution and average cloud droplet sizes without appreciably altering the liquid water content (LWC). Particle scattering efficiencies are related to the size parameter, x, defined above in Eq. (3). The scattering efficiencies of these droplets for 0.6 micrometer radiatioq (x = 42 and 31 for 4 and 3 micrometer droplets, respectively) are near 2.0. as shown in Fig. 8. Therefore, for 0.6 micrometer radiation, there is little difference in the scattering efficiencies between 4 and 3 micrometer cloud droplets.

For a cloud with a constant LWC, a decrease in the average r means the number of smaller particles increases. From Eq. (2), the decreasing cross sectional areas will be partly compensated for by the increased numbers of particles. This effect is an integrated effect of all the droplet radii. The specific size distributions in the ship track and adjacent regions are not known; thus this effect cannot be quantitatively analyzed at this time. However, there are no obvious visible effects (such as ship tracks)

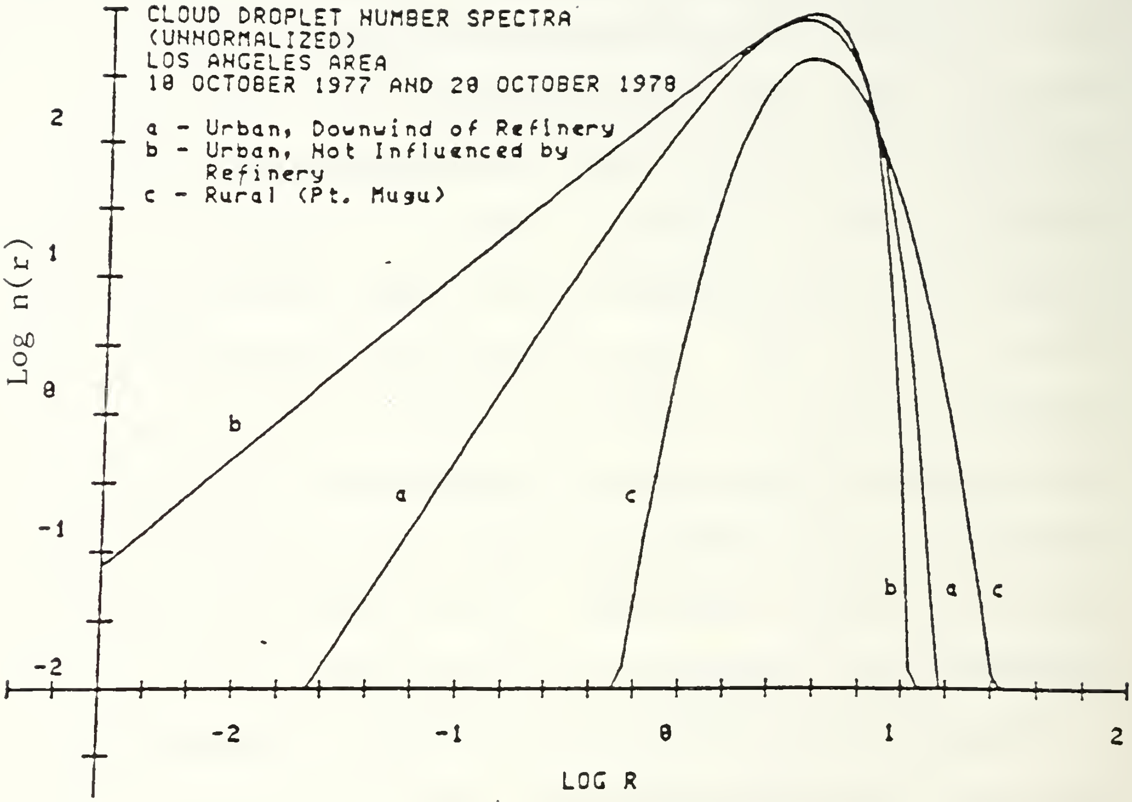

Fig. 9. The cloud droplet size distribution log n(r) vs. log (radius) (from Barrett, et al., 1979).

in band 1 or 2 imagery in this case to suggest this qualitative analysis is in error. Band 2 radiation processes are similar to band 1 processes. The above discussions generally apply also to band 2. The sensed radiation in bands 1 and 2 only consists of reflected or scattered solar radiation.

Band 4 radiation (11 micrometers) is due to emitted thermal radiation. According to Table 2, the solar component of 11 micrometer radiation is less than 1% of the emitted terrestrial radiation. Additionally, at the band 4 and 5 wavelengths, clouds are nearly black bodies and absorb 99% of band 4 and 5 radiation reaching them (d'Entremont, 1985.) Therefore, the amount of solar radiation in bands 4 and 5 that clouds reflect is less than 0.001% of their total radiance, since they emit band 4 and 5 radiation as black bodies. The emission curves in Fig. 7 show that the terrestrial emission has its maximum at about 10 micrometers. The band 4 or 5 radiance sensed at a satellite is thus composed of emitted thermal radiation with essentially no reflected solar radiation.

Over open oceans, clouds above the surface will generally be colder than the sea surface. At 11 micrometers the emissivity of the sea surface is greater than 98% (Hobson and Williams, 1971). Since both clouds as well as the sea surface are nearly black bodies at 11 micrometers, the colder clouds will emit less radiation than the sea

surface. As mentioned above, colder features appear brighter in IR images than warmer features. This usually makes clouds appear light against the earth's darker surface.

The single scattering albedo is defined as the probability that a photon will be scattered instead of absorbed if it interacts with a particle. Liquid water has a single scattering albedo of about 1 for radiation in bands 1 and 2 (Irvine and Pollack, 1968). There is essentially no chance that a water droplet will absorb an incident 0.6 micrometer photon. Thus, band 1 radiation will continue to scatter after entering a cloud until it is scattered out of the cloud. Therefore, It can penetrate very thick clouds after many scattering events. Since the total extinction is the sum of the scattering and absorption extinctions, clouds have lower extinctions when viewed in bands 1 or 2 than in bands 3, 4 or 5 which have lower single scattering albedos and thus absorb more radiation (Bohren and Huffman, 1983). Clouds thus appear "thinner" than they do in bands 3, 4 or 5.

Band 4 and 5 radiation has a single scattering albedo for water droplets of about 0.2 (Irvine and Pollack, 1968). Therefore, a photon has a 80% chance of absorption at each interaction and only a few interactions will result in a high rate of absorption. Thus, there is very little chance for band 4 or 5 radiation to penetrate more than a few

meters through a cloud. The sensed radiation in bands 4 and 5 originates from within the top few meters of the cloud and is related to the temperature of very nearly the cloud top.

III. CAUSES OF ANOMALOUS EFFECTS IN BAND 3

Band 3 radiation effects are caused by the same physical process as those of bands 1, 2, 4 and 5. However, the main source of band 1 and 2 effects, reflection, is different than the source of bands 4 and 5 effects, thermal emission. In band 3, both reflection and thermal emission of radiation are important.

A. APPARENT CLOUD TOP/SEA SURFACE RADIANCE REVERSAL

The clear atmosphere is nearly transparent at 3.7 micrometers. Fig. 10 shows an atomspheric window from about 3.5 to 4.1 micrometers. Water vapor doesn't significantly attenuate the signal in band 3, especially above the cloud top level where water vapor decreases throughout the rest of the atmosphere.

A cloud's reflectivity is related to its scattering optical depth. The scattering optical depth, τ, is equal to

$$\tau = \int_0^\infty b \, dz. \qquad (4)$$

A cloud's reflected radiance will increase if its scattering optical depth is increased without increasing its absorptivity. This can be accomplished by the addition of

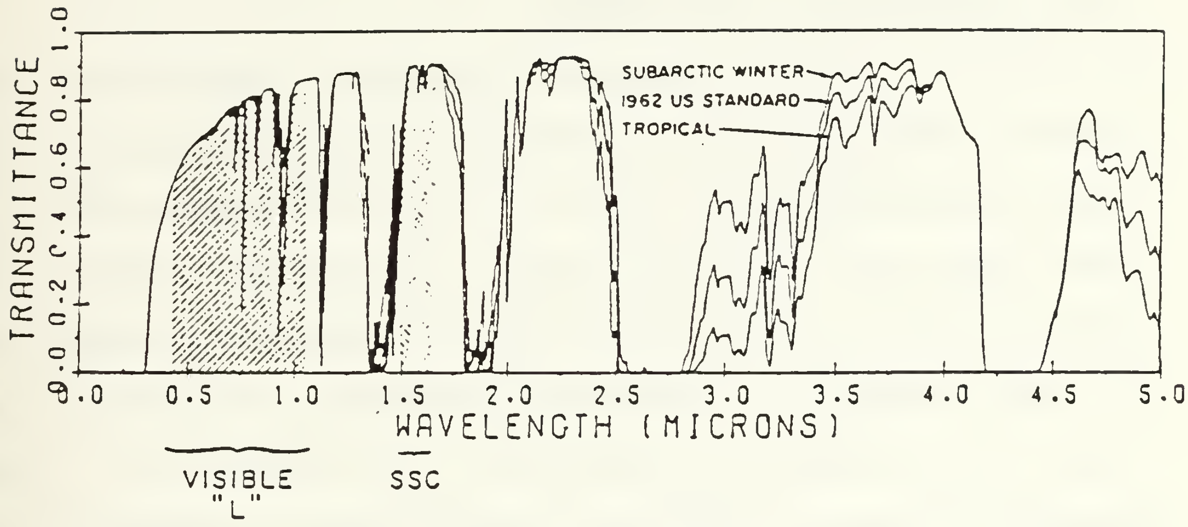

Fig. 10. Atmospheric spectral transmission from visible to near infrared wavelengths. Band 3 lies at 3.7 micrometers, in the 3.4 to 4.1 micrometer "window" (from Bunting and d'Entremont, 1982).

moisture, leading to an increase in LWC. However, from Eq. (2), increasing the LWC would increase the reflectivity at all wavelengths, since if the relative size distribution of cloud droplets remained unchanged there would be more droplets or if some of the droplets become larger to accommodate the increased moisture the radii would increase. This is not seen in bands 1 or 2. Therefore, the LWC of the clouds is probably not being changed significantly in the ship tracks by the ship exhaust.

Table 3 gives calculated radiances recieved at the satellte from two standard surfaces, the sea-surface and the top of a thin stratus layer. The solar radiance value is from Table 2. The cloud albedos come from Coakley and Davies (1985). Using Hunt's (1973) value for the emissivity of thin clouds and a standard temperature, a value for the total cloud radiance is obtained. The reflectivity of the sea-surface is 1 minus the absorptivity (or emissivity). Using the sea-surface emissivity of Warnecke _et al_. (1969), and the calculated values of reflectivity and a standard sea-surface temperature, the radiance recieved from the sea-surface is calculated.

According to Table 3, even though cloud tops may be many degrees colder than the sea surface, when they have a sufficiently high albedo they may reflect enough additional solar radiation to have a higher radiance than the sea surface. Bell and Wong (1981) described clouds with tops 34

K colder than the underlying sea-surface that appeared warmer than the surface due to scattered band 3 solar radiation.

TABLE 3

SOURCE OF SENSED BAND 3 RADIANCE VALUES

(radiance values in W/m^2 sr cm)

	Sea-Surface	Thin Clouds
Solar radiance	38900	38900
Albedo (%)	7	12
Reflected radiance	2680	4670
Emissivity (%)	93	56
Temperature (K)	290	280
Emitted radiance	2400	952
Total sensed radiance	5080	5622

Another unique band 3 effect resulting from the interaction of reflected solar radiation with emitted terrestrial radiation is very low radiance received from ice clouds. Ice clouds are strong absorbers of band 3 radiation; Hunt (1973) gives an absorptivity of 0.894 for thin (optical depth of 5) and 0.985 for thicker (optical depth 10) clouds. Thus, cirrus clouds would be expected to absorb much of the incident solar band 3 radiance. Since they are thin, they would tramsmit much of the remaining radiance, leaving very little radiance to be reflected back

to the satellite sensor. The ice clouds would also be colder than the lower water clouds, so they would emit less radiance than the lower clouds and the surface. Therefore, they would appear much less radiant than water clouds. The high clouds at the bottom of Fig. 5 are, in fact, much lighter (much less radiant) than the lower clouds.

B. ANOMALOUS SHIP TRACKS

As mentioned above, there has been little attention to date given to the band 3 unique ship track phenomenon. The ship tracks appear to be warmer than the surrounding clouds. However, band 4 temperature calculations from the measured radiance of the clouds show the clouds to be of nearly uniform temperature. There is no significant evidence of ship tracks in the band 4 derived temperature fields. Using the above radiance reversal reasoning they must have higher albedos at 3.7 micrometers or much higher emissivities than the surrounding cloud.

If the emissivity increased in band 3, it would result in an increased emission from the clouds, thus increasing their emitted brightness. This is not likely since an increased emissivity is equivalent to an equal increase in the cloud's absorptivity. This would reduce the reflected solar radiation, which, as is discussed above, is often the dominant source of cloud radiance that the satellite measures.

Comparing bands 1 and 3 (Figs. 1 and 5) indicates the ship tracks occur in thin clouds. Hunt (1973) gave an emissivity for clouds with an optical depth of 5 (which is an optically thin cloud) of 0.559 in band 3. If, in an extreme case, the emissivity of the cloud were raised to 1, the emitted radiation from a 280 K cloud would increase from 894 to 1600 W/m^2 sr cm, a change of 706 W/m^2 sr cm. If a conservative reflectivity of .10 is used for the initial cloud and 0 for the final cloud (since the absorptivity is also raised to 1), the reflected solar band 3 radiance would be reduced from 3890 to 0 W/m^2 sr cm. Thus, the cloud would appear much cooler than the adjacent clouds, instead of warmer. Thus, an increase in emissivity is probably not the cause of the apparently warm ship tracks.

If the so called "ship tracks" are, in fact, caused by exhaust from passing ships, they are probably the result of the introduction into the atmosphere of something that alters the microphysical properties of the clouds. The high temperature of the exhaust probably is not the cause of the effect. The ship tracks persist for hours or days but an exhaust plume would rise (due to its density being less than the cooler surrounding air) to a level where it attained thermal equalibrium. According to the Davidson-Bryant plume rise formula (Stern _et al_., 1973), a 600 K plume exiting a 5 m stack at 15 m/s into an ambient wind of 10 m/s would rise about 53 m above the top of the stack. This is well below

the cloud top height for most marine stratus. After the plume reaches 53 m, it assumes the same temperature as the surrounding air. Further, as mentioned above, there is no increase in thermal radiation observed in band 4 at the ship track locations. Thus, the most likely origin of the ship tracks is that they are a manifestation of the pollutants in the exhaust; specifically, the suspended particulates.

The Study of Critical Environmental Problems (1970) mentioned by Twomey (1977) referred to the possibility that polluted cloud droplets would be stronger absorbers than unpolluted cloud droplets. The study concluded that the increased absorptivity would result in more absorption of visible wavelength energy by the clouds. This would increase the cloud's temperature, thus increasing the amount of emitted energy at 3.7 micrometers. However, as mentioned above, this would also result in increased thermal emissions in band 4 and 5. There is no evidence of the ship tracks in band 4. Probably it would also result in a reduced reflection of the solar band 3 radiance, offsetting the increase in absorptivity (and thus emissivity). Therefore, if this is occurring, it does not appear to be a significant contributer to the band 3 ship tracks.

In Figs. 1 through 5, the clouds in the area located southwest of Point Conception are thinner than those in the surrounding areas. In the band 3 imagery in Fig. 5, this is the bright patch (thus "cooler" clouds) with crossed, dark

("warmer") ship tracks. From Table 2, band 3, incoming solar radiation is, for high sun angles, up to 24 times as intense as emitted terrestrial radiation. As discussed above, the low, thick stratus clouds off the coast near Point Conception look warmer than the sea surface since they are strongly scattering solar radiation. As can be seen in the band 3 image (Fig. 5) as the low stratus clouds became thinner, their albedo (and thus the solar radiation scattered from them) decreases. Therefore, the clouds appear cooler as they get thinner. Ship tracks through a "thin" area are dark in the displayed image of band 3 like the adjacent thick clouds. This, with the above emittance arguments, implies that the ship tracks are areas of increased cloud albedo in band 3. As mentioned below, increased albedos can be caused by increasing optical depth, other parameters remaining the same. The anomalous ship tracks are not visible in band 1 or 2 image because the albedo is not increased in bands 1 or 2.

Twomey (1977) concluded that adding pollution increases the number of droplets in a cloud by increasing the number of smaller droplets at the expense of larger droplets. This is due to the addition of condensation nuclei by the pollution. He then showed that this causes an increase in the cloud's albedo, by increasing the scattering in the cloud. Twomey determined that the increased absorption due to the added pollutants would be a secondary effect until

the cloud's optical depth became very large. He showed that the absorption only becomes important when a cloud's optical depth exceeds 30 to 200, depending on cloud type. He concluded that for most clouds, the increasing optical depth of the cloud due to the added pollutants tends to increase the cloud's albedo more than the pollution would increase its absorptivity.

Barrett et al. (1979) showed that polluted urban clouds have higher numbers of aerosols, and thus droplets, than unpolluted marine clouds with a similar LWC. The increased number of aerosols increases the available condensation nuclei, thus altering the size distribution of the droplets toward a larger number of smaller droplets. As mentioned above, he found the mean radii of the droplets in clouds containing refinery effluents was measured to be 3 micrometers and the mean size in unpolluted marine stratus clouds was 4 micrometers.

As developed in Chapter 2, scattering is a function of cross section area, the size distribution, and the scattering efficiency, Q(m,r). The average droplet cross sectional areas would reduce due to injected pollutants, such as might be found in a ship's exhaust plume, adding condensation nuclei. This results in more, but smaller, droplets, thus altering the shape of the size distribution. The assumption is made that the LWC does not significantly change. These two effects, altering the area and size

distribution, tend to offset each other. The effect that produces ship tracks is probably not due to the increased number of droplets alone, since this would also increase the visible scattering. There is generally no evidence of ship tracks in either bands 1 or 2 in these cases.

The scattering efficiency is a function of x (Eq. 3), which, in turn, is a function of the droplet radius and wavelength. Even though the size distributions measured by Barrett et al. (1979) are not the same as those in and near the ship tracks, the general sizes of the measured droplets are probably fairly representative of sizes of the ship track areas. If they are, the values for x of the average size droplets would probably range from 4 to 8.

Fig. 8 shows that these values of x yield scattering efficiencies on the region of the curve where the value of Q(m,r) exibits the greatest variability. The values of the droplets are average radii which may not be representative of the best value to characterize the average scattering efficiencies for the two distributions. The distributions may not be representative of the actual ambient conditions. However, for the droplet sizes to remain on the most variable part of the efficiency curve, the droplets radii must vary such that x varies from about 2 to 10. This implies a desirable average effective droplet size range of from 1.2 to 5.9 micrometers.

The reason for the relative brightness of the ship tracks is increased reflectance of band 3 solar radiance due to the increased scattering by cloud droplets. The most likely reason for the increased scattering is the increase of the scattering efficiency due to a shift in the effective droplet size. This occurs because the droplet size distribution is modified toward greater numbers of smaller particles as the ship's exhaust injects additional condensation nuclei into the cloud layer.

IV. BAND 3 ANALYSIS ALGORITHMS

Each pixel in the AVHRR data contains values for each of the five bands for digital display. Bands 1 and 2 provide values of albedo (reflected radiance divided by incoming solar radiance). Bands 3, 4 and 5 contain radiance values. All bands are digitized for display with values of 0 for black through 1023 for white. Using calibration coefficients allows the retrieval of the actual radiance or albedo values. (Bunting and d'Entremont, 1982.)

Several steps were utilized to analyze the data in the three cases. First, the raw display data were formatted for display on a system with 256 shades of grey. Then, the band 4 value for each pixel was calibrated to yield a radiance. The radiance was then inserted into an inverted Planck function (for band 4) to yield the pixel temperature. Fig. 11 is the resulting band 4 temperature display. The grey scale is reversed on Fig. 11, cold is black and warm is white. Notice the lack of ship track effects or variation across the stratus cloud deck.

The pixel temperatures were used in the Planck function for band 3 to obtain band 3 emitted radiance values. The band 3 emitted radiance values were then converted to displayable form. Fig. 12 is an image of the band 3

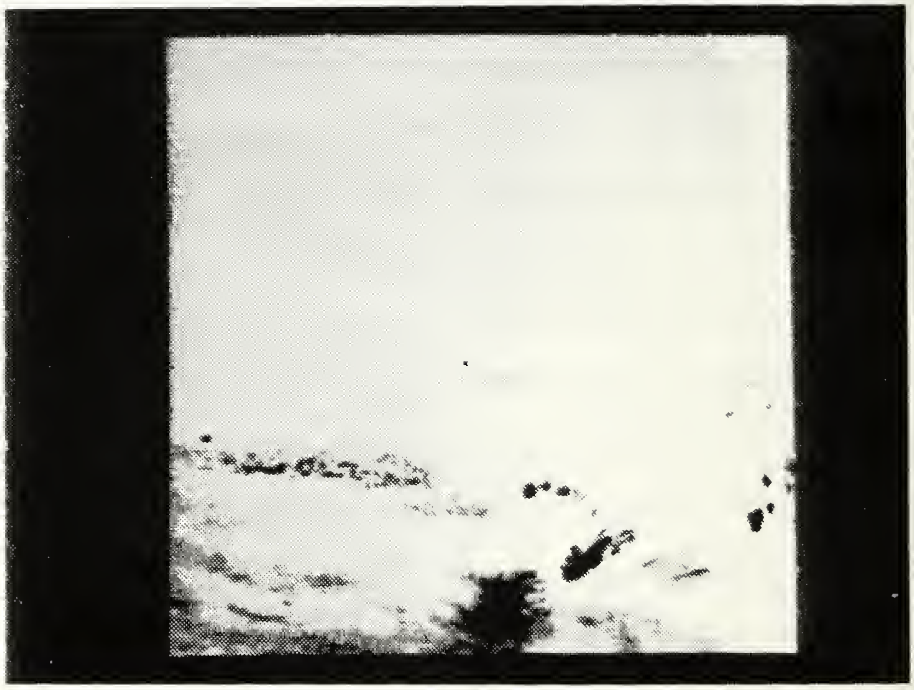

Fig. 11. AVHRR modified image, location and date same as Fig. 1. Pixel band 4 radiance values converted to temperatures and displayed.

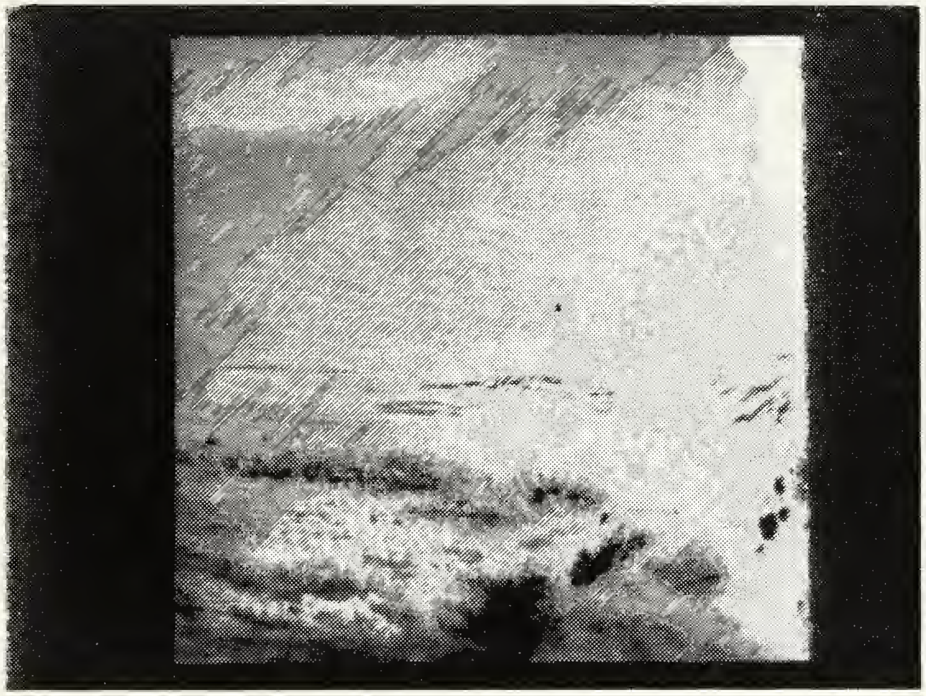

Fig. 12. Same as Fig. 11, band 3 pixel radiance emission values calculated from band 4 temperature values.

emissions. The band 3 calculated emitted radiance values for each pixel were then subtracted from the corresponding calibrated band 3 observed pixel radiance values. This yields an image of band 3 reflected values as is shown in Fig. 13. The reflected values are estimated values, since the emittance values of the ship tracks at 3.7 micrometers are uncertain. The emittance in the algorithm is assumed to be 1. The emittance values for oceans are from 0.97 to 0.93 (Warnecke et al., 1969). Hunt (1973) calculated emissivities, for clouds with a mean droplet radius of 4 micrometers in band 3, of from 0.0610 to 0.5767 for clouds with optical depths of 1 to 10, respectively. This algorithm is not sophisticated enough to distinguish cloud optical depths or even cloud versus non-cloud sources.

Finally, the albedos of the band 3 pixels' reflected radiances were determined (by dividing by a reference observed solar radiance, calculated from Thekaekara et al., 1969). These values were divided by the band 2 calibrated albedos for the source pixels. This was done to highlight areas where the band 3 albedos varied from a close correspondence with band 2 albedos. Fig. 14 is an example of this analysis.

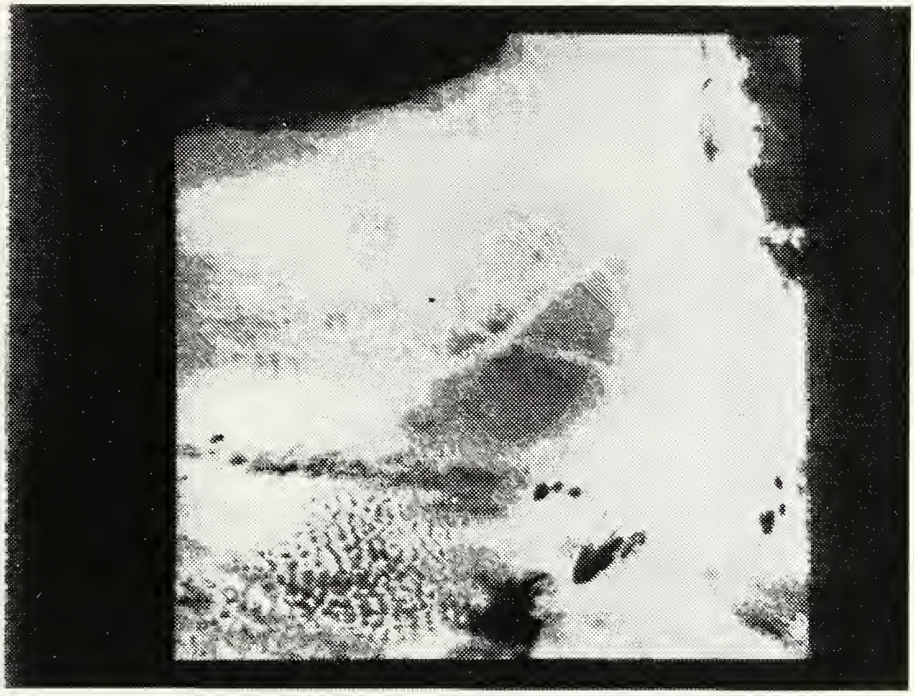

Fig. 13. Same as Fig. 11, band 3 reflected solar radiance. From observed band 3 pixel radiance with calculated emitted band 3 radiance subtracted out.

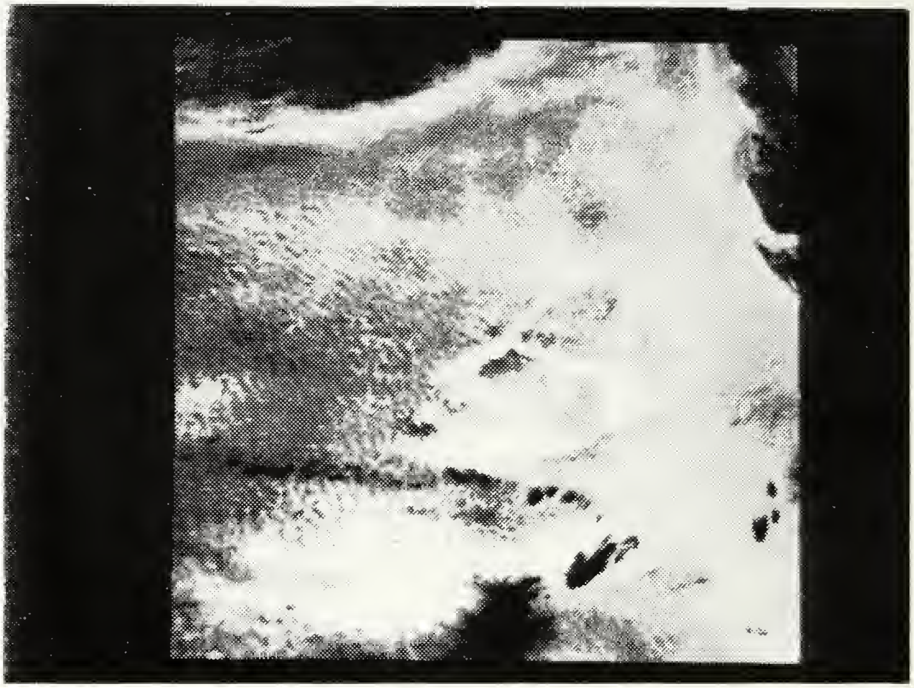

Fig. 14. Scene same as Fig. 1. Displayed ratio of band 3 albedo to band 2 albedo.

V. BAND 3 ANALYSES

Three cases of AVHRR data will now be examined with the algorithms presented in Chap. IV. Then a tentative analysis technique will be discussed.

A. CASE 1

The first set of data are from the marine area off the southern California coast, taken by NOAA 9 on 3 April 1985, at about 1400 LST. Fig. 6 is an overview scene of the received band 1 data. The full resolution series (1 km) of data (512 X 512 image) are centered on the relatively clear patch southwest of Point Conception.

Fig. 1 is the band 1 full resolution image of the area. The land surface in the top right corner is free of cloud cover. The clear ocean is visible in the top left corner; there is a patch of scattered clouds in the center of the image. The cloud deck appears to be stratocumulus with some higher clouds at the bottom of the image. There is an area of fog or stratus near the coast and along the right edge of the image. Fig. 2, the band 2 image, appears similar to Fig. 1 except the land surface is better defined, as is discussed below.

Figs. 1 and 2 illustrate the effect of reflected solar radiation well. Areas of low reflectivity (or albedo)

absorb most of the incident solar radiation. The oceans strongly absorb the solar radiation so they appear very dark. The land surfaces also strongly absorb band 1 solar radiation, as in Fig. 1. However, the land features have a higher reflectivity in band 2; therefore, in Fig. 2 the land image is lighter and more detail is visible in it. Clouds reflect strongly in both band 1 and band 2, thus they are bright.

Figs. 3 and 4 are representative of band 4 and 5 imagery, respectively. There are no apparent differences between bands 4 and 5 imagery, as shown in Figs. 3 and 4. However, water vapor more strongly absorbs band 5 radiation than band 4 radiation (McMillin, 1975). Thus, the differences in actual radiance values allow inferences to be made about the water vapor content of the atmosphere. This aids in correcting satellite sensed sea-surface temperature values. However, in this area of imagery, there is generally a strong subsidence above the surface; this implies that there is very little moisture above the subsidence inversion. The inversion is usually near the tops of the clouds. Thus, one would not expect to observe any significant visual differences between Figs. 3 or 4. Band 4 imagery will be discussed below; the discussion also applies to band 5.

Fig. 3 is typical of band 4 imagery. The sensed band 4 radiation is essentially all thermally emitted radiation.

In the early afternoon, the land surface in early spring is usually warmer than the sea-surface. It thus appears much darker than the sea. The land-surface temperature, as calculated from values measured in band 4, varies from 295 K to over 300 K. These land surface temperatures seem plausible for early afternoon in April in California. The air at the surface of the ocean is often nearly the same temperature as the sea surface. However, as one senses higher into the atmosphere, the temperatures are generally cooler. The low clouds on most of the image appear nearly the same shade of gray as the sea surface; since both the clouds and sea surface have emissivities of nearly 1 they must, therefore, be nearly the same temperature. The sea-surface temperature determined from band 4 radiance is very uniform at from 284 K to 285 K. The low clouds exhibit slightly more variability, being mostly 282 K to 283 K with occasional 1 K warmer or cooler areas. This indicates the height of the top of the clouds is very uniform and low.

The small clouds in the lower portion of the picture are considerably brighter than the underlying surface. They must be much colder, and therefore higher, than the lower clouds. The temperature of the high clouds exhibits wider variability; their temperatures range from 233 K to 242 K. This indicates that they are much higher than the lower cloud deck and their height varies from cloud to cloud. The

warm temperature, thus the low height, of the main cloud deck therefore means, comparing bands 1 and 4 (Figs. 1 and 3) that the main cloud deck is a low stratocumulus deck.

Fig. 5 presents the band 3 imagery. The effects of both reflection and emission are evident. The land surface emits and reflects band 3 radiation more strongly than the sea surface. It thus appears darker than the sea just to the south of the area of land or the sea in the top left corner.

The clouds both reflect and emit band 3 radiation. Therefore, the reflected radiation adds to the radiance emitted from the top of the cloud. The sum of these two radiance sources is then sensed by the satellite. If a cloud's albedo is high enough, the cloud will appear darker (warmer) than the adjacent sea surface. Most of the clouds in Fig. 5 are much darker (appear much warmer) than the sea surface, which is actually one to 1 K to 3 K or more warmer than low cloud tops. If the cloud tops of the stratus deck in the image were black body emitters, the emitted band 3 radiance sensed at the satellite indicate their temperatures would be 310 K to 312 K. This is 25 K to 28 K warmer than the underlying sea surface.

The crossed ship tracks in the center of Fig. 5 imply an altered state of the microphysics of the clouds. They do not appear in the visible imagery, nor do they appear to have different temperatures in the band 4 or 5 imagery. Table 4 compares ship track radiance values to adjacent area

radiance values in bands 2, 3 and 4 and in the reflected component of band 3. The table values are averages of eight pairs of ship track and adjacent, non-ship track values of individual pixel radiances in each band and from the band 3 reflected radiance pixel calculations.

There is a small increase in radiance in band 2, a moderate increase in band 3, a very small decrease in band 4 and a large increase in the reflected band 3 energy. The increase in band 2 reflectivities may be due to slight imbalances in the change in droplet size distribution and cross sectional areas. However, there is not enough large scale organization of the effect for ship tracks to be visually apparent. If changes are to occur in band 4, the expected change would be a slight decrease in element radiances. Since the elements are above the surface in an area of scattered clouds, they would absorb upwelling surface radiation and radiate at cooler temperatures. The result would be less surface contaminating radiance reaching the satellite. Since there are few clouds visible in band 2, there are few radiating elements, therefore the net reduction of surface contamination would be slight.

TABLE 4

COMPARISON OF AVERAGE SHIP TRACK AND ADJACENT AREA RADIANCES

(band 2 values are albedos normalized to 100;

radiance values are in $mW/m^2\ sr\ cm^{-1}$)

Case 1	Band 2	Band 3	Band 4	Band 3 refl.
Ship Tracks	17.9	1.016	86.4	0.741
Std. Dev.	2.26	0.060	0.33	0.065
Adjacent	17.2	0.719	86.5	0.454
Std. Dev.	5.28	0.141	0.80	0.139
Average Increase (%)	4.0	42.6	-0.05	62.9

The increase in band 3 radiance agrees very well with the observed imagery since ship tracks are readily observable. According to the argument for cloud reflectance increases in Chapter 3, the changing droplet size distributions are strongly increasing the scattering, thus the received band 3 radiance is significantly increased. Larger scale support for the scattering mechanism is observable along the right edge of the band 1, 2 and 3 imagery. The individual cloud elements blend into a more homogeneous mass of cloud. They also reflect more radiance in bands 1, 2 and 3. This is likely due to the advection of continental aerosols into the marine environment. The aerosols are providing many more nuclei than the unpolluted

maritime air. Therefore, many more droplets are produced, enhancing scattering in bands 1, 2 and 3.

Comparing the band 2 image and the reflected band 3 radiance image (Figs. 2 and 13) illustrates the differences in the aerosol distributions and the effect of the differences on the apparent edge of the continental aerosols. The enhanced reflection is farther westward and more extremely enhanced in Fig. 13 than in Fig. 1. Averages of radiance values of points were calculated from the main marine stratus deck into the area of apparent continental aerosol effects. The radiance in band 2 increases about 38%, and band 3 total radiance increases 50% while band 4 doesn't change significantly. The band 3 reflected radiance increases by about 79%. The band 2 radiance increases above the mean levels much closer to the coast (farther east) than does band 3.

A possible reason for the visible channel effect of the continental aerosols but not in the ship track case is that the continental case would provide many more aerosols than a single ship. This would more efficiently shift the droplet size distribution toward small, much more numerous drops, since there would be a much larger number of available condensation nuclei competing for the available moisture. Thus, the cross sectional area decrease would be over-compensated for by the increased numbers of droplets.

B. CASE 2

The second case investigated is also off the west coast of the United States. The pass was recorded at 1400 LST, on 4 April 1985, by NOAA 9, and a band 2 overview is presented in Fig. 15. The area of interest is the center of the top edge of the imagery; it is presented in full resolution by Fig. 16.

There are three items of interest in Fig. 16. Notice the V-shaped ship tracks in the upper right corner, this time present in band 1 and 2 data. Conover (1969) described visible ship tracks. He hypothesized three conditions required for the production of visible ship tracks: 1) a low level, convectively unstable layer capped by a stable layer, 2) saturation or slight supersaturation near the top of the layer, and 3) a deficit of cloud condensation nuclei in the layer. A passing ship would then inject enough nuclei to trigger formation of the cloud bands. These bands have been observed to be up to 500 km long and 25 km wide. The hypothesized conditions were observed to occur in regions where the visible ship tracks occur in 1967 and 1968. In 1969, a weather reconnaissance aircraft observed a wide stratus band and followed it to its source, a ship. The ship was "physically forming a cloud trail which appeared much like a ship's wake at the surface" according to the report of the flight crew. (Conover, 1969).

Fig. 15. AVHRR band 2 area overview, 1400 LST, 4 April 1985. Image of Pacific Coast of United States and Baja California. Full resolution image area indicated by box.

Fig. 16. Full resolution subscene of Fig. 15, band 2.

The band 3 image of the same scene is presented in Fig. 17. Notice that the visible ship tracks appear as a fuzzy dark V shaped pattern. At the bottom center of the image is a distinct image of an anomalous ship track. It appears to be newly formed since it is narrow, has sharp boundaries and tapers to a definite point. The ship forming it is probably heading north, toward the intersection of the two visible ship tracks. Band 2 (Fig. 16) shows no trace of the ship track.

The numerical values for Case 2 are given in Table 5 and are produced in the same way as Table 4 values. 15 values along the ship track were averaged together. Then 15 values on each side of the ship track (30 total) were averaged together. The ship track occurs along the edge of the cloud field visible in Fig. 15. This is the reason for the large increase in band 2 albedos in Table 5. The average of the 15 values along the cloudy edge adjacent to the ship track was 0.7% more than the average of the ship track values. The average of the 15 values along the clear edge adjacent to the ship track was 41% less than the average of the ship track values. This is to be expected since the ship track was nearly at the edge of the existing cloud field.

Fig. 17. Same as Fig. 16, band 3.

TABLE 5

COMPARISON OF AVERAGE SHIP TRACK AND ADJACENT AREA RADIANCES

(band 2 values are albedos normalized to 100;

radiance values are in mW/m^2 sr cm^{-1})

Case 2	Band 2	Band 3	Band 4	Band 3 refl.
Ship Tracks	37.5	0.527	81.6	0.286
Std. Dev.	14.7	0.024	0.63	0.026
Adjacent	32.2	0.415	82.1	0.166
Std. Dev.	13.5	0.044	1.08	0.047
Average Increase (%)	12.6	27.1	-0.07	71.4

The band 4 imagery presented in Fig. 18 again show evidence of the visible ship tracks but not of the anomalous band 3 ship track. The visible ship tracks are at nearly the same temperature as the surrounding sea surface, indicating it consists of a very low cloud. In band 2, the visible ship tracks are nearly 95% brighter than their surroundings. The band 3 ship track is only 22% brighter. However, the reflected radiance in band 3 for the visible ship track shown in Fig. 19 is 85% brighter than the surrounding sea surface.

The final item of interest is the bright west edge of the cloud field in the band 3 reflected radiance image (Fig. 19). However, when compared with the band 2 image (Fig. 16) the eastern edge of the cloud field is sharply defined but

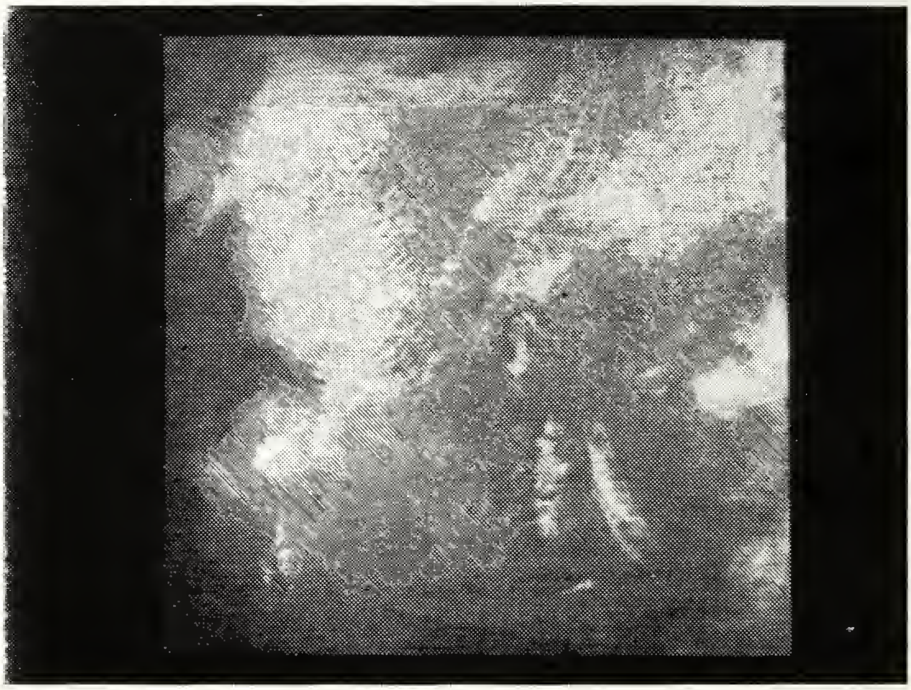

Fig. 18. Same as Fig. 16, band 4.

Fig. 19. Same as Fig. 16, modified imagery displaying band 3 reflected solar radiation, as in Fig. 13.

the western edge is diffuse with poorly defined elements. The cause of the bright western edge may be due to the size distribution of the cloud droplets. The western edge of the cloud may consist of thin stratus cloud or thin fog with a distribution of smaller droplets. The cloud elements away from the western edge of the cloud field seem to be more convective in nature; they would thus have larger droplets (Hunt, 1973 and Coakley and Davies, 1985). Thus, the western edge droplet size distribution would be skewed toward smaller droplets, possibly enhancing the scattering efficiency of the cloud edge (by changing x, as on Fig. 8). Since the cloud is thin and diffuse, the size of particles also may be reduced due to evaporative effects.

C. CASE 3

The first two cases containing anomalous ship tracks were located over oceans. Case 3 was an attempt to identify anomalous ship track-type phenomena over the continental United States. Fig. 20 presents an overview of the eastern United States in band 1. The location of the area of study is just northwest of the head of the comma cloud marking the passage of a weather disturbance. The southern end of Lake Michigan is visible and is the center of the full resolution NOAA 9 imagery. The date is 8 April 1985 at about 1400 LST.

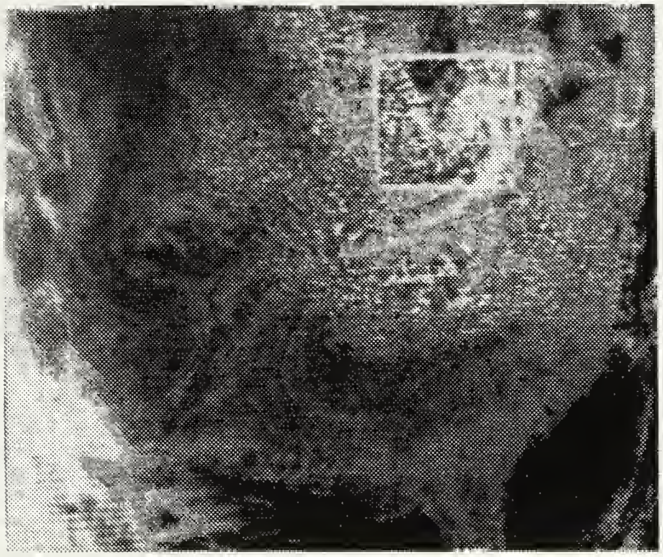

Fig. 20. AVHRR band 2 area overview. 1400 LST, 8 April 1985. Image of eastern United States from north Florida to southern Great Lakes. Full resolution image area indicated by box.

Fig. 21 is the band 2, 1 km resolution imagery of the Case 3 area of interest. The head of the comma cloud is clearly visible. It is composed of high clouds, possibly cirrus clouds, due to clusters of thunderstorms. There are numerous convective clouds dominating the image with some possible enhanced convection along the southwest shore of the lake. Over Lake Michigan cloud streaks or visible ship tracks are present. However, if there are any city pollution plume tracks (an analog of ship tracks) on the land, they are not apparent due to widespread convective activity. There are numerous, naturally occurring lines of cumulus in the image.

The band 3 imagery are shown in Fig. 22. The lake is bright, as is the top of the comma cloud and some of the plumes from the enhanced cumulus. That indicates, again, that the lake absorbs the incoming radiation and its emitted radiation, though greater than the clouds, is less than the clouds' total emitted and reflected radiance. The most important features this image illustrates are the very bright (thus cold) clouds. The bright clouds in the comma cloud head are probably glaciated cloud tops from the convective disturbances in the comma head. The enhanced convection cloud tops along the southwest shore of the lake are also probably glaciated. As described in Chap. III, frozen clouds are very strong absorbers of band 3 radiation, thus they do not reflect as much incoming solar band 3

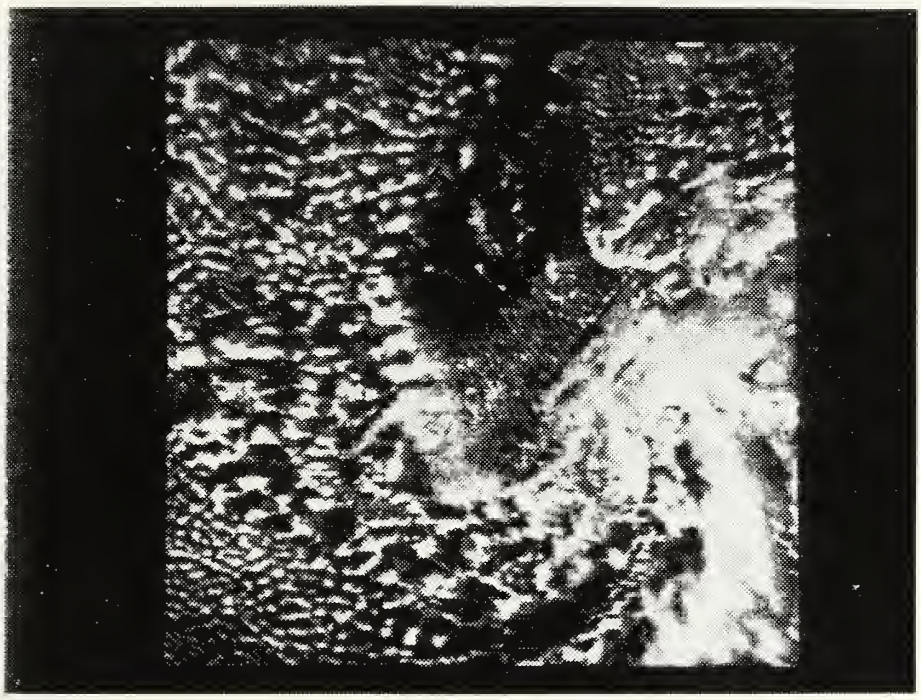

Fig. 21. Full resolution subscene of Fig. 20, band 2.

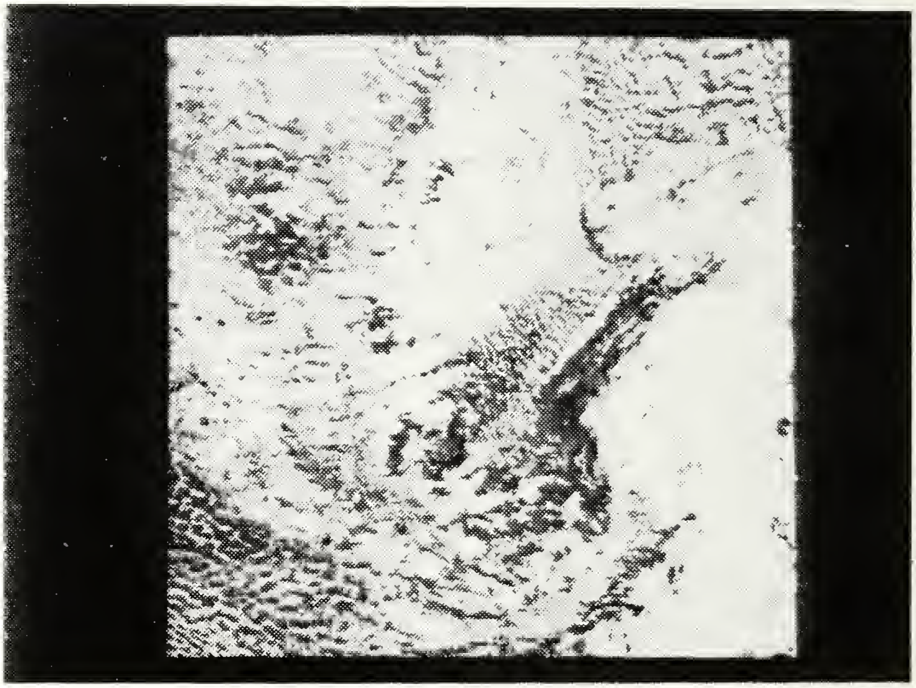

Fig. 22. Same as Fig. 21, band 3.

radiance as liquid clouds. However, the lower clouds reflect the incoming band 3 solar radiation effectively enough to appear warmer than the land or lake surface below them. Therefore, the lower cumulus clouds appear darker (warmer) than the underlying land and water, and much darker than the glaciated clouds.

Band 4 imagery are presented in Fig. 23. It indicates that the top of the comma is very cold and some of the enhanced convection clouds are also quite cold (they are bright). The water and land are warmer than the clouds, as in the other cases.

Fig. 24 is the reflected band 3 imagery. The top of the comma head reflects much less radiance than the lower clouds; therefore, it is glaciated. Some of the enhanced convection also appears to be glaciated. Other than the glaciated clouds, the reflected band 3 image (Fig. 24) looks very much like the band 2 imagery (Fig. 21).

D. REFLECTANCE RATIO

To highlight areas where the reflectance of band 3 is significantly different than band 2, the band 3 albedo was divided by the band 2 albedo for each pixel. The resulting values were then converted for display. Bright areas are those where the ratio is greater than about 0.7 and dark areas are where the ratio is less than about 0.3. The only areas the ratio exceeds 1 are those areas where there is a

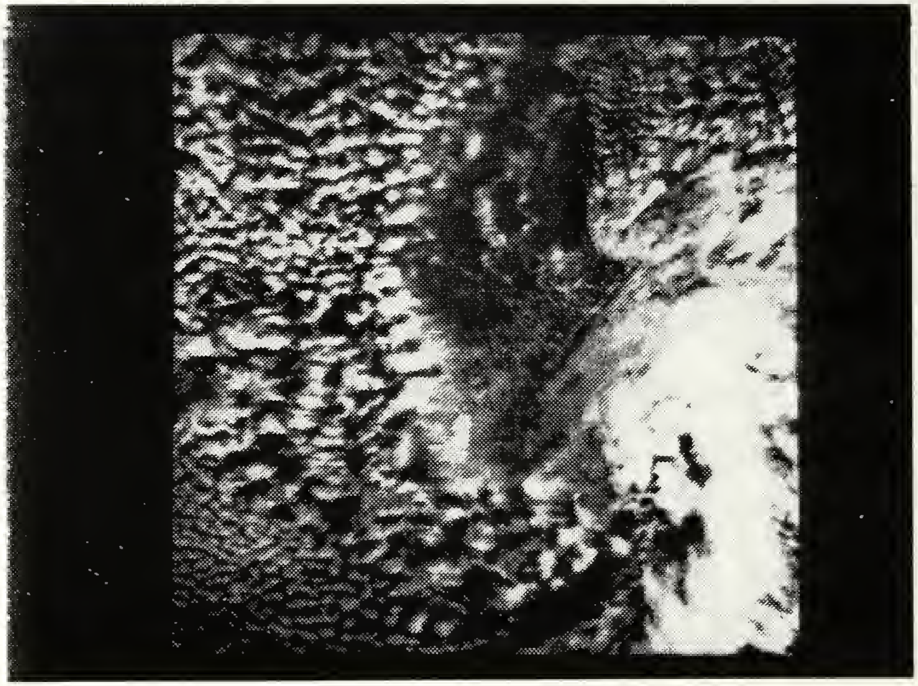

Fig. 23. Same as Fig. 21, band 4.

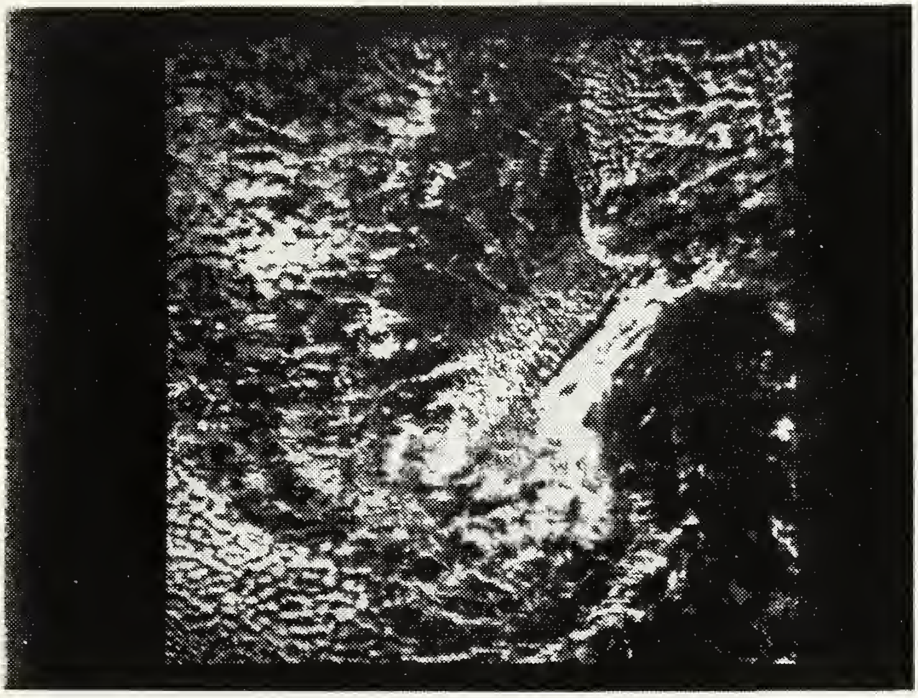

Fig. 24. Same as Fig. 21, modified imagery displaying band 3 reflected solar radiation, as in Fig. 13.

definite image in band 3 and not one in band 2, such as in the Case 1 ship tracks. The very dark areas are where there is a strong band 2 radiance and the reflected band 3 image is suppressed, such as in the glaciated cloud tops.

The ratio of the imagery analysis of Case 1 is shown in Fig. 14. The ship tracks are bright and the edge of the continental aerosol effect is bright. These effects were expected. However, the areas where the ship tracks cross are now very bright. This is because there is very little band 2 radiance being returned from the ship track areas since the cloud cover in the area consists of scattered, small cumulus clouds. However, there is apparently enough moisture present, possibly in the form of a light, moist haze, to return significant band 3 reflected radiance. The edge enhancement occurs at the north edge of the cloud field where the clouds become thin and less cumuliform. Thus, the cloud droplets might be expected to be smaller due to entrainment of dry air and the subsequent evaporation of the droplets. The high clouds are accented by being very dark. This enhancement technique seems to have worked well for Case 1.

The ratio image for Case 2 is presented in Fig. 25. The visual ship tracks are barely visible as slightly darker than the surrounding imagery. Analyzing the data for the visible ship tracks, the visible channel had a greater increase in brightness (94.5%) than band 3 (22%). Thus, the

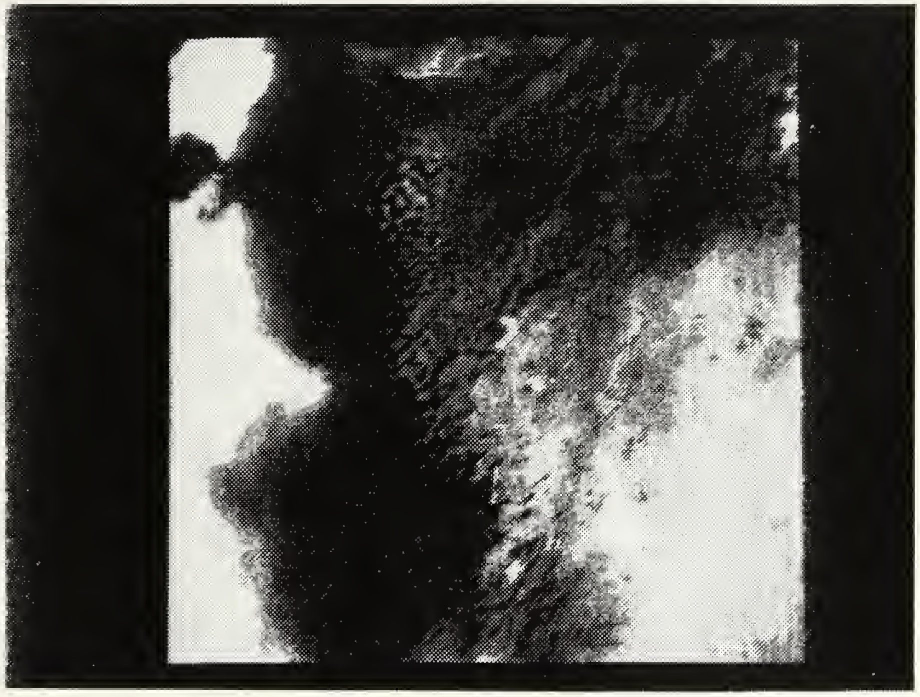

Fig. 25. Scene same as Fig. 16, Case 2.
Displayed ratio of band albedo to band 2 albedo.

ratios result in a slightly reversed (darker) image. However, there is no indication of the anomalous ship track. Possibly it was a ship track that was enhanced in band 3 and hidden in band 2 in the cloud edges. However, due to the distinctness of the band 3 anomalous ship track, this does not seem likely. The western edge of the image is very bright. Possibly this is an area of sun glint in band 3. There is also a moderately brighter area in the lower right corner, which is an area of mostly clear skies. This technique does not work well for ship tracks in Case 2. However, it does highlight other areas of interest, such as areas of thin or very thin clouds.

Fig. 26 is the ratio image from Case 3. The glaciated clouds are further enhanced compared to the reflected band 3 radiance image in Fig. 24. The enhanced convection area is more sharply defined. There are additional areas of brightness in the lake area, around the visible cloud lines, again possibly indicating areas of non-visible small droplet concentration.

This technique seems particularly well suited to observing areas of limited cloudiness where there might be a non-visible fog or other scattering source. It also accentuates areas of glaciation, thus being possibly useful to detect ice clouds and their relation to thunderstorms. Finally, as is particularly noticeable in Case 3 (Fig. 26), convective cloud elements are highlighted by a bright

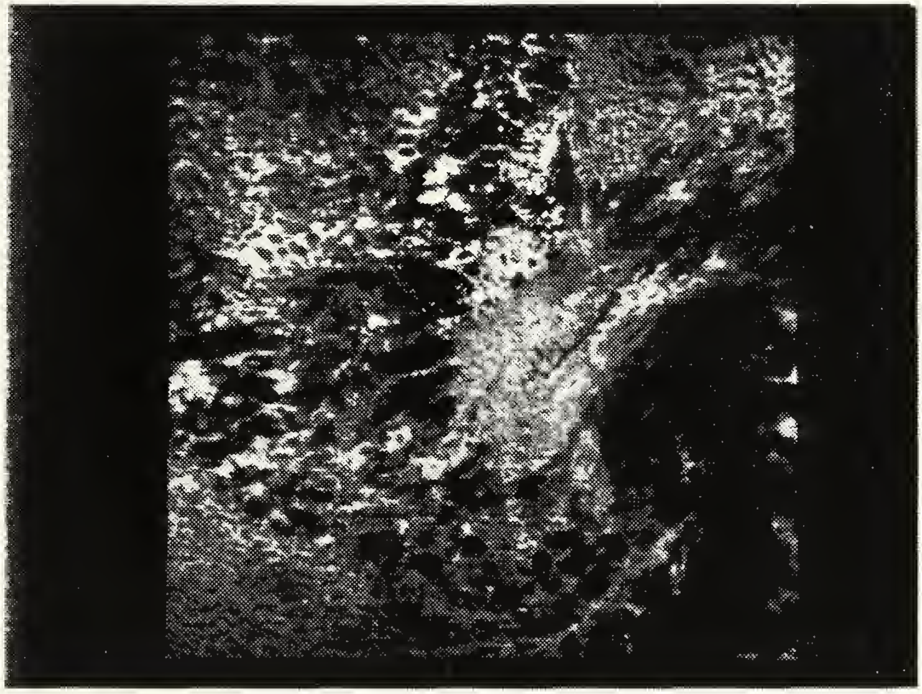

Fig. 26. Scene same as Fig. 21, Case 3, image displayed as Fig. 25.

ring around each element. This occurs some in Case 1 (Fig. 14) and almost not at all in Case 2 (Fig. 25). This may be due to evaporative effects at the cloud edges thinning out the clouds, much as is occurring at the edges of the cloud fields except on a smaller scale.

VI. CONCLUSION

The anomalous features in band 3 are due to the addition of reflected solar radiance to the radiance emitted thermally in band 3. Striking examples of the apparent reversal of cloud top and sea-surface temperatures are observed in Case 1. The cloud tops are 1 K to 3 K or more cooler than the adjacent sea surface. However, the cloud radiances in band 3 are much higher than the sea-surface radiances. The cloud radiances, if they were due only to black body emission, would indicate cloud top temperatures of about 310 K to 312 K, which is 25 K to 28 K warmer than the sea surface. This is in agreement with the Bell and Wong study (1981).

The ship track phenomena are probably not due to increases of emission due to increased temperatures or emissivities. Band 4 imagery indicate essentially no change in temperature at the ship tracks. An increase in emissivity would also be equivalent to an increase in absorptivity. The net result would be an increased absorption of band 3 solar radiation which would reduce the reflected solar band 3 radiance. Since the reflected portion of the band 3 radiance is as significant as, or more significant than, the emitted radiance in band 3, the ship

tracks would not be visible or would be brighter (low radiance) instead of darker (high radiance).

Therefore, the cause of the ship tracks is due to an increase of the reflectivity of the clouds which results in increased radiance being sensed by the satellite. The increased reflectivity is due to an increase in the scattering of the band 3 radiation by the cloud. This is most likely due to an increase in the scattering efficiency of the cloud droplets. The number of droplets also increase, but their cross sectional areas are reduced. These two effects nearly counteract each other in the ship track phenomena. If they did not compensate, scattering would also increase in the visible region by a significant amount, as is the case in case 1 where the continental aerosols force large shifts in the size distributions. The resulting increased reflection is not observed in band 1 or 2 despite the fact that the tracks occur in areas where the visible radiation reflectance is sensitive to optical depth. The reasons the anomalous ship tracks do not become visible ship tracks may be because they occur in areas that do not have a deficit of nuclei. There are clouds already present in the areas of the anomalous band 3 ship tracks which indicate that there are enough condensation nuclei present to form clouds.

The bright areas around the edges of individual clouds and the edges of cloud fields may be due to a deficit of

large droplets and an excess of smaller droplets due to evaporation. These features are strikingly apparent in imagery where the ratio of reflectances in band 3 to band 2 displayed.

These anomalous band 3 phenomena are newly observed. The data available at this time are limited to remotely sensed satellite imagery. Thus, it is necessary to perform in situ measurements to verify or refute the microphysical assumptions of this thesis. It is important to verify that ships do, in fact, produce the "ship tracks." The particular types of weather required to produce ship tracks also would be useful to know.

Using band 3 daylight imagery, especially when it is analyzed in relation to other imagery, may allow the development of a global climatology of cloud types and their microphysical properties. The spectral optical depths of clouds might be able to be determined if a better understanding of these phenomena is attained. These ideas were suggested by Twomey and Cocks (1982). These methods could also provide detection of ice clouds. It might also allow determination of the areal coverage of small thunderstorms, as in Fig. 26, the albedo ratio image of case 3. The water available in clouds too thin to detect in bands 1 or 4 also might be detected by these procedures. Thus, a more accurate determination of the liquid water content in sparsely clouded regions would be available.

City smoke or effluent plumes might be expected to produce "pollution tracks" when viewed under suitable conditions (daylight, after a frontal passage replaces the local stagnant air). Tracking these pollutant plumes is an important problem and this may be an easy method to obtain plume tracking data in cloudy cases.

Day time band 3 imagery have the potential to provide new data on the structure of clouds, and the distribution of cloud types, especially if the data are combined with the other AVHRR bands' data in multispectral analysis.

LIST OF REFERENCES

Barrett, E. W., F. P. Parungo and R. F. Pueschel, 1979: Cloud modification by urban pollution: a physical demonstration. Meteorol. Rdsch., 32, 136-149.

Bell, G. J., and M. C. Wong, 1981: The near-infrared radiation received by satellites from clouds. Mon. Wea. Rev., 109, 2158-2163.

Bohren, C. F., and D. R. Huffman, 1983: Absorption and Scattering of Light by Small Particles. Wiley and Sons, New York, 530 pp.

Bunting, J. T., and R. P. d'Entremont, 1982: Improved Cloud Detection Utilizing Defense Meteorological Satellite Program Near Infrared Measurements. Air Force Geophysics Laboratory, Hanscom AFB, MA, AFGL-TR-82-0027, 91 pp.

Coakley, J. A., and R. Davies, 1985: The effect of cloud sides on reflected solar radiation as deduced from satellite observations. Submitted to J. Atmos. Sci.

Conover, J. H., 1969: New observations of anomalous cloud lines. J. Atmos. Sci., 26, 1153-1154.

d'Entremont, R. P., 1985: Low and mid-level cloud analysis using nighttime multispectral imagery. Submitted to J. Clim. and Appl. Meteor.

Fett, R. W., P. E. LaViolette, M. Nestor, J. W. Nickerson and K. Rabe, 1979: Navy Tactical Applications Guide, Volume II: Environmental Phenomena and Effects. Department of the Navy, Washington, D. C., Naval Environmental Prediction Research Facility Technical Report 77-04, 161 pp.

Friedlander, S. K., 1977: Smoke, Dust, and Haze. Wiley and Sons, New York, 317 pp.

Hobson, D. E., and D. Williams, 1971: Infrared spectrum reflectance of sea water. Appl. Optics, 10, 2372-2373.

Hunt, G. E., 1973: Radiative properties of terrestrial clouds at visible and infra-red thermal window wavelengths. Quart. J. R. Met. Soc, 99, 346-359.

Irvine, W. M., and J. B. Pollack, 1968: Infrared optical properties of water and ice spheres. Icarus, 8, 324-360.

Kidwell, K. B., 1984: NOAA Polar Orbiter Data (TIROS-N, NOAA-6, NOAA-7, and NOAA-8) Users Guide. National Oceanic and Atmospheric Administration, NESDIS, Washington, D. C., 148 pp.

McMillin, L. M., 1975: Estimation of sea surface temperatures from the infrared window measurements with different absorption. J. Geophys. Res, 80, 5113-5117.

Stern, A. C., H. C. Wohlers, R. W. Boubel and W. P. Lowry 1973: Fundamentals of Air Pollution. Academic Press, New York, 492 pp.

Sellers, W. D., 1965: Physical Climatology, University of Chicago Press, Chicago, 272 pp.

Study of Critical Environmental Problems, 1970: Mass Impact On the Global Environment. The MIT Press, Cambridge, MA, 319 pp.

Thekaekara, M. P., R. Kruger and C. H. Duncan, 1969: Solar irradiance measurements from a research aircraft. Appl. Optics, 8, 1713-1732.

Twomey, S., 1977: The effect of pollution on the shortwave albedo of clouds. J. Atmos. Sci., 34, 1149-1152.

Twomey, S., and T. Cocks, 1982: Spectral reflectance of clouds in the near-infrared: comparison of measurements and calculation. J. Meteor. Soc. Japan, 60, 583-592.

Warnecke, G., L. M. McMillin and J. L. Allison, 1969: Ocean Current and Sea Surface Temperature Observations from Meteorological Satellites. National Aeronautics and Space Administration, NASA TN D-5142, 46 pp.

INITIAL DISTRIBUTION

		No. Copies
1.	Defense Technical Information Center Cameron Station Alexandria, VA 22304-6145	2
2.	Library Code 0142 Naval Postgraduate School Monterey, CA 93943-5002	2
3.	Chairman (Code 63Rd) Department of Meteorology Naval Postgraduate School Monterey, CA 93943	1
4.	Professor P. A. Durkee (Code 63De) Department of Meteorology Naval Postgraduate School Monterey, CA 93943	10
5.	Professor C. H. Wash (Code 63Wx) Department of Meteorology Naval Postgraduate School Monterey, CA 93943	1
6.	Captain John M. Rogers 8 Dick Phelps Road Watsonville, CA 95076	1
7.	Director Naval Oceanography Division Naval Observatory 34th and Massachusetts Avenue NW Washington, DC 20390	1
8.	Commander Naval Oceanography Command NSTL Station Bay St. Louis, MS 39522	1
9.	Commanding Officer Naval Oceanographic Office NSTL Station Bay St. Louis, MS 39522	1
10.	Commanding Officer Fleet Numerical Oceanography Center Monterey, CA 93940	1

11.	Commanding Officer Naval Ocean Research and Development Activity NSTL Station Bay St. Louis, MS 39522	1
12.	Commanding Officer Naval Environmental Prediction Research Facility Monterey, CA 93940	1
13.	Chairman, Oceanography Department U. S. Naval Academy Annapolis, MD 21402	1
14.	Chief of Naval Research 800 N. Quincy Street Arlington, VA 22217	1
15.	Office of Naval Research (Code 420) Naval Ocean Research and Development Activity 800 N. Quincy Street Arlington, VA 22217	1
16.	Program Manager (CIRF) Air Force Institute of Technology Wright-Patterson Air Force Base, OH 45433	1
17.	Commander Air Weather Service Scott Air Force Base, IL 62225	1
18.	Commanding Officer Air Force Global Weather Central Offutt Air Force Base, NE 68113	1
19.	Commander (AIR-370) Naval Sir Systems Command Washington, DC 20360	1

Thesis
R68537 Rogers
c.1 Investigation of anomalous cloud features in 3.7 micrometer satellite imagery.